Preclinical evaluation of BAY 1075553, a novel F-18-labelled inhibitor of prostate-specific membrane antigen for PET imaging of prostate cancer

ARTICLE *in* EUROPEAN JOURNAL OF NUCLEAR MEDICINE · AUGUST 2013

Impact Factor: 5.38 · DOI: 10.1007/s00259-013-2527-3 · Source: PubMed

Eur J Nucl Med Mol Imaging
DOI 10.1007/s00259-013-2527-3

ORIGINAL ARTICLE

Preclinical evaluation of BAY 1075553, a novel ^{18}F-labelled inhibitor of prostate-specific membrane antigen for PET imaging of prostate cancer

Ralf Lesche · Georg Kettschau · Alexey V. Gromov · Niels Böhnke · Sandra Borkowski · Ursula Mönning · Christa Hegele-Hartung · Olaf Döhr · Ludger M. Dinkelborg · Keith Graham

Received: 26 February 2013 / Accepted: 25 July 2013

Abstract
Purpose Prostate-specific membrane antigen (PSMA) is a transmembrane protein overexpressed in prostate cancer and is therefore being explored as a biomarker for diagnosing and staging of the disease. Here we report preclinical data on **BAY 1075553** (a 9:1 mixture of (2*S*,4*S*)- and (2*R*,4*S*)-2-[^{18}F]fluoro-4-phosphonomethyl-pentanedioic acid), a novel ^{18}F-labelled small molecule inhibitor of PSMA enzymatic activity, which can be efficiently synthesized from a direct radiolabelling precursor.
Methods The ^{18}F-radiolabelled stereoisomers of 2-[^{18}F]fluoro-4-(phosphonomethyl)-pentanedioic acid were synthesized from their respective isomerically pure precursors dimethyl 2-{[bis(benzyloxy)phosphoryl]methyl}-4-(tosyloxy) pentanedioate. In vivo positron emission tomography (PET) imaging and biodistribution studies were conducted in mice bearing LNCaP, 22Rv1 and PC-3 tumours. Pharmacokinetic parameters and dosimetry estimates were calculated based on biodistribution studies in rodents. For non-clinical safety assessment (safety pharmacology, toxicology) to support a single-dose human microdose study, off-target effects in vitro, effects on vital organ functions (cardiovascular in dogs, nervous system in rats), mutagenicity screens and an extended single-dose study in rats were conducted with the non-radioactive racemic analogue of **BAY 1075553**.
Results **BAY 1075553** showed high tumour accumulation specific to PSMA-positive tumour-bearing mice and was superior to other stereoisomers tested. Fast clearance of **BAY 1075553** resulted overall in low background signals in other organs except for high uptake into kidney and bladder which was mainly caused by renal elimination of **BAY 1075553**. A modest uptake into bone was observed which decreased over time indicating organ-specific uptake as opposed to defluorination of **BAY 1075553** in vivo. Biodistribution studies found highest organ doses for kidneys and the urinary bladder wall resulting in a projected effective dose (ED) in humans of 0.0219 mSv/MBq. Non-clinical safety studies did not show off-target activity, effects on vital organs function or dose-dependent adverse effects.
Conclusion **BAY 1075553** was identified as a promising PET tracer for PSMA-positive prostate tumours in preclinical studies. **BAY 1075553** can be produced using a robust, direct radiosynthesis procedure. Pharmacokinetic, toxicology and safety pharmacology studies support the application of **BAY 1075553** in a first-in-man microdose study with single i.v. administration.

Keywords Molecular imaging · PET · Prostate cancer · Prostate-specific membrane antigen · ^{18}F

Electronic supplementary material The online version of this article (doi:10.1007/s00259-013-2527-3) contains supplementary material, which is available to authorized users.

R. Lesche (✉) · G. Kettschau · A. V. Gromov · N. Böhnke · S. Borkowski · U. Mönning · O. Döhr · L. M. Dinkelborg · K. Graham (✉)
Global Drug Discovery, Bayer Healthcare, Berlin, Germany,
Muellerstrasse 178, 13342 Berlin, Germany
e-mail: ralf.lesche@bayer.com
e-mail: keith.graham@bayer.com

C. Hegele-Hartung
Global Drug Discovery, Bayer Healthcare, Wuppertal, Germany,
Aprather Weg 18a, 42096 Wuppertal, Germany

Present Address:
L. M. Dinkelborg
Piramal Imaging GmbH, Tegeler Weg 6-7, 13353 Berlin, Germany

Introduction

Prostate cancer remains the second leading cancer found in men. In the USA alone more than 217,000 new cases were

Published online: 17 August 2013

diagnosed and approximately 32,000 prostate cancer-related deaths were recorded in 2010 [1]. Serum-based prostate-specific antigen (PSA) screening for prostate cancer is well established in the USA and is gaining more acceptance in Europe. However, the PSA test, while being fairly sensitive, lacks specificity resulting in a mandatory follow-up examination by prostate biopsy procedures to manifest the diagnosis. Because it is serum based the PSA test lacks anatomic resolution of the location and the extent of the individual lesion. As a consequence prostate biopsy procedures are set up to randomly target the prostate with up to 20 needle cores, but still miss the tumour in a substantial number of cases often leading to re-biopsy procedures. To improve the diagnostic accuracy of prostate biopsies several radiotracers are currently being explored to image prostate cancer patients. [^{11}C]Choline and [^{18}F]fluorocholine have been used mainly for imaging of metastatic prostate cancer. Specialized centres, predominantly located in Europe, have demonstrated good diagnostic performance of choline-based positron emission tomography (PET) tracers in detecting recurrent prostate cancer with sensitivity values up to 80 % at high specificity [2, 3] and similar performance values were reported for [^{11}C]acetate [4]. However, sensitivity values seem to depend on PSA values of the patient at presentation [5]. Recently, [^{18}F]fluorocholine received regulatory approval in selected European countries for evaluating prostate cancer metastases [6]. While significant advances were reported in the characterization of metastatic prostate tumours, a convincing benefit for diagnosing and staging primary prostate cancer patients remains to be demonstrated. Only a subset of primary prostate tumours was shown to be avid for [^{18}F]fluorodeoxyglucose (FDG) uptake, likely due to the slowly growing nature of these tumours [7]. This is in line with a recent report showing preferential uptake of [^{18}F]FDG into more aggressive forms of prostate tumours [8]. Choline-based tracers on the other hand were reported to lack specificity to differentiate malignant from benign disease such as benign prostatic hyperplasia and prostatitis when used to evaluate organ-confined disease (reviewed in [9]) [10]. As a consequence a high medical need remains to locate malignant tumours in the prostate for precise biopsy guidance and to allow for lymph node evaluation with high diagnostic performance.

Recently, progress has been made in identifying membrane-based proteins specifically overexpressed in prostate cancer and with low background in other organs [11]. Among those targets prostate-specific membrane antigen (PSMA) has attracted significant attention due to its reported high overexpression in a majority of primary and metastatic prostate cancer patients [12–20]. Overexpression of PSMA was found to be even more pronounced in more aggressive tumours including lymph node metastases [15] as well as upon androgen deprivation [17]. In normal human tissues, PSMA expression was found at low to modest levels in the prostate, brain, proximal tubules of the kidney and intestinal brush border membranes [14, 21]. Due to its favourable expression profile as a biomarker for prostate cancer, antibodies targeting PSMA were developed for molecular imaging. Currently the only US Food and Drug Administration approved radiopharmaceutical for imaging prostate cancer is ^{111}In-labelled capromab pendetide (ProstaScint, Cytogen, Princeton, NJ, USA), a radiolabelled antibody targeting PSMA. However, the ProstaScint antibody, which targets the intracellular PSMA domain, has had limited clinical use due to its slow distribution and clearance, which contribute to difficulties in image interpretation [22]. J591, an antibody targeting an extracellular epitope of PSMA, has entered clinical trials as a radiotherapeutic agent for metastatic castration-resistant prostate cancer [23]. Attempts to label J591 with radioisotopes suitable for diagnostic purposes have been reported and showed promise in preclinical studies [24]. Before PSMA found widespread attention for its prostate cancer overexpression, the protein had previously and independently been characterized in brain tissue as carboxy peptidase II [25] and highly potent compounds inhibiting its *N*-acetylated alpha-linked acidic dipeptidase (NAALAdase) activity have been reported [26]. Recently, a number of groups have started to investigate small molecule PSMA inhibitors radiolabelled with either PET or single photon emission computed tomography (SPECT) radioisotopes [27–31] for imaging prostate cancer and first compounds have proceeded into clinical testing [32, 33].

Herein, we report on the direct radiosynthesis and preclinical characterization of the stereoisomers of 2-[^{18}F]fluoro-4-(phosphonomethyl)-pentanedioic acid and identify **BAY 1075553** as a promising PET tracer for further testing in clinical trials (Fig. 1).

Materials and methods

Reagents

The non-radioactive [^{19}F] reference compounds **1**, **2**, **3**, **4** and **5** were synthesized as previously described [34]. **1** was used as a mixture of stereoisomers for non-clinical safety studies. 2-(Phosphonomethyl)pentanedioic acid (2-PMPA) was purchased from Tocris. AG11A8 resin was purchased from BioRad. All other chemicals were purchased from Sigma-Aldrich and were American Chemical Society (ACS) or HPLC grade unless specifically stated.

Preparative and analytical methods–chiral preparative HPLC Preparative HPLC method 1: CHIRALCEL OD-H 5 μm column (250×20 mm) with a flow rate of 20.0 ml/min at ambient temperature using UV detection at 210 nm. The solvent system used was isocratic (hexane:ethanol 85:15);

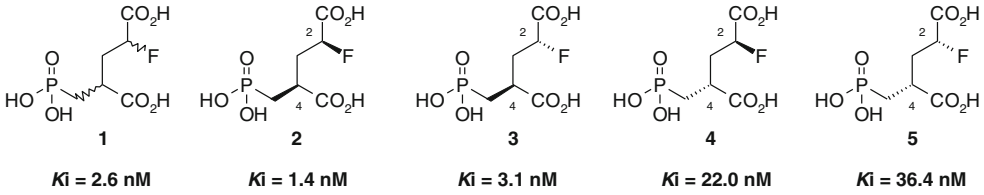

Fig. 1 Stereoisomers of 2-fluoro-4-phosphonomethyl-pentanedioic acid and their binding affinities

preparative HPLC method 2: CHIRALPAK IA 5 μm column (250×30 mm) with a flow rate of 25.0 ml/min at ambient temperature using UV detection at 210 nm. The solvent system used was pure ethanol.

Radiochemistry analytics Analytical HPLC chromatograms were obtained using an Agilent 1100 system with ChemStation software, equipped with UV multi-wavelength, Corona charged aerosol detector (CAD) and Raytest Gabi Star detectors. Semi-preparative HPLC purifications were carried out as indicated. The semi-preparative HPLC system used was a Merck-Hitachi L6200A system equipped with a Knauer variable wavelength detector and an Eberline radiation detector.

Synthesis of precursors 6, 7, 8 and 9 as single stereoisomers Tosylate precursor **6** was prepared as an isomeric mixture as reported previously [34]. Separation into its four stereoisomers was accomplished by chiral preparative HPLC on an OD-H phase according to preparative HPLC method 1 specified above. For larger-scale isolation of the (2*S*,4*R*) precursor isomer **7** leading predominantly to the stereoisomer of the (2*S*,4*S*) radiotracer **BAY 1075553** featuring the highest tumour uptake, it turned out advantageous to switch to an IA stationary chiral HPLC phase (preparative HPLC method 2). In either method, **7** was the first isomer to elute and **8** was second. The two isomers with the 2*R* configuration could only be separated using preparative HPLC method 1 as they co-eluted using preparative HPLC method 2 (for details regarding analytical procedures refer to [35]). The absolute configuration of the respective precursor isomers is in line with an S_N2 inversion at C-4 during nucleophilic displacement of the tosylate by fluoride and is supported inter alia by nuclear Overhauser effect (NOE) MRI studies on suitable derivatives of isomerically pure synthetic intermediates in the synthesis of **7–10**, and by correlations with the corresponding stereoisomers of **2–5** [35], the absolute configuration of which has been assigned by means of X-ray crystallography [34]. The reader is referred to the fact that, in order to obey chemical naming rules, the atom numbering of the pentadioic acid backbone reverts from **6** to **1** as a result of protecting groups removal, i.e. C-4 bearing the tosylate leaving group in the precursor species **6–10** correlates to C-2 bearing the fluoride in the radiotracer species **BAY 1075553**, **[^{18}F]3** and **[^{18}F]5**.

Radiosynthesis of BAY 1075553, a 9:1 mixture of (2S,4S)-2-[^{18}F]fluoro-4-(phosphonomethyl)-pentanedioic acid ([^{18}F]2) and (2R,4S)-2-[^{18}F]fluoro-4-(phosphonomethyl)-pentanedioic acid ([^{18}F]3) [^{18}F]Fluoride (12 GBq) was immobilized on a preconditioned QMA (Waters) cartridge (preconditioned by washing the cartridge with 5 ml 0.5 M K_2CO_3 and 10 ml water). The [^{18}F]fluoride was eluted using a solution of Cs_2CO_3 (2.3 mg) in 500 μl water and K_{222} (5.0 mg) in 1,500 μl acetonitrile. This solution was dried at 120 °C with stirring under vacuum, with a stream of nitrogen. Additional acetonitrile (1 ml) was added and the drying step was repeated. A solution of **7** (4 mg) in polymerase chain reaction (PCR) grade dimethyl sulphoxide (DMSO, 500 μl) was added and heated at 120 °C for 15 min. The mixture was diluted with 20 ml water and passed through a C18 light Sep-Pak (preconditioned with 5 ml ethanol and with 10 ml water). The Sep-Pak was washed with 5 ml water and eluted with 1 ml MeCN. The eluted solution was diluted with 3 ml water and purified over semi-preparative HPLC [ACE 5 μm C18, 250×10 mm, isocratic 60 % MeCN in 40 % water+0.1 % trifluoroacetic acid (TFA), flow 4 ml/min]. The product peak was collected and diluted with 20 ml water and passed through a C18 light Sep-Pak (preconditioned with 5 ml ethanol and with 10 ml water). The Sep-Pak was washed with 5 ml water and was eluted with 1 ml ethanol. The ethanol solution was dried under gentle N_2 stream for 10 min at 90 °C; 500 μl 6 M HCl was added and the mixture was incubated for 10 min at 120 °C. After cooling the reaction mixture was diluted with 1 ml water and passed through a cartridge containing AG11A8 resin (ion retardation resin, ~11 g, preconditioned with 200 ml saline) connected in series with a C18 light Sep-Pak (preconditioned with 5 ml ethanol and with 10 ml water). The cartridges were then washed with saline (5 ml) and eluents were collected to give **BAY 1075553** (978 MBq, 17 % d.c.). The radiochemical purity was >95 % as analysed by thin-layer chromatography (TLC) [silica: *n*-butanol:acetic acid:ethanol:H_2O (12:3:1.5:5)] and HPLC (ZIC-HILIC 5 μm 100×4.6 mm 200 Å; solvent A: 0.1 M ammonium formate in water pH 3.2; solvent B: acetonitrile; gradient 70 % B for 5 min, 70 % B to 10 % B in 1 min, 10 % B for 2 min, 10 % B to 70 % B in 1 min, 70 % B for 2 min; flow 2.0 ml/min; detection: radioactive detector, Corona CAD detector) (see Supplementary Figure 2). In order to determine the ratio of the different stereoisomers in the final formulated solution a derivatization method was developed to generate the tetrakis-

methyl ester derivative which could be analysed by chiral HPLC [36, 37]. This derivatization method determined that the final formulated product contained ca. 90 % of (2*S*,4*S*)-2-[^{18}F]fluoro-4-(phosphonomethyl)-pentanedioic acid (**[^{18}F]2**) and ca. 10 % of (2*R*,4*S*)-2-[^{18}F]fluoro-4-(phosphonomethyl)-pentanedioic acid (**[^{18}F]3**).

Radiosynthesis of (2R,4S)-2-[^{18}F]fluoro-4-(phosphonomethyl)-pentanedioic acid ([^{18}F]3) [^{18}F]3 was synthesized via an unoptimized analogous method with the precursor **8** in 6 % d.c. yield. The extent of epimerization was not determined as the derivatization method was developed after the head-to-head comparison was carried out.

Radiosynthesis of (2R,4R)-2-[^{18}F]fluoro-4-(phosphonomethyl)-pentanedioic acid ([^{18}F]5) [^{18}F]5 was synthesized via an unoptimized analogous method with the precursor **10** in 16 % d.c.y. The extent of epimerization was not determined as the derivatization method was developed after the head-to-head comparison was carried out.

Animals All animal experiments were performed in compliance with the current version of the German law on the Protection and Welfare of Animals. Mice and rats were kept under normal laboratory conditions at a temperature of 22± 2 °C and a dark/light rhythm of 12 h. Food and water were provided ad libitum. Acclimation period was at least 6 days before the beginning of a study. Male Balb/c nude mice (Charles River, Sulzfeld, Germany) were used for subcutaneous inoculation of human LNCaP xenografts. A testosterone pellet (total dose 12.5 mg/pellet, release time 90 days; Innovative Research of America, Cat.# NA-151) was implanted 3–4 days before inoculation of tumour cells. LNCaP (human prostate cancer) tumour cells (1×10^7 cells per animal in 100 μl Matrigel™) were injected subcutaneously into the right flank and allowed to grow for approximately 4 weeks. Male NMRI nude mice (Taconic, Ejby, Denmark) were inoculated with 22RV1 (5×10^6 cells per animal in 100 μl Matrigel™) and PC-3 cells (2×10^6 cells per animal in 100 μl Matrigel™), respectively, and allowed to grow for approximately 3 weeks. Male NMRI mice were used for the dosimetry study and male Wistar rats (Hsd CpB:Wu; Harlan GmbH) for kinetics and extended single-dose toxicity studies, respectively. Male and female Beagle dogs were used for safety pharmacological studies. The dogs were anaesthetized initially with thiopental. Anaesthesia was maintained with droperidol/fentanyl/nitrous oxide and animals were ventilated artificially with a mixture of O_2 and N_2O.

Biodistribution studies

Biodistribution experiments were performed using nude mice bearing human LNCaP tumours and non-tumour-bearing NMRI mice. Animals were injected i.v. with 250 kBq of **BAY 1075553** in 100 μl saline. The animals were sacrificed at different time points (from 0.25 to 4 h, $n=3$ for each time point) post-injection (p.i.). Organs and tissues of interest were collected and weighed. The amount of radioactivity was determined in a gamma counter to calculate the uptake (% injected dose per gram tissue).

In vivo PET/CT studies

Conscious animals were injected i.v. with 7–10 MBq of PET tracer, anaesthetized shortly before scanning and scanned in a whole-body configuration from 50 to 70 min p.i. and 110 to 130 min p.i., respectively, in the small animal PET/CT system Inveon (Siemens, Knoxville, TN, USA). Settings for CT were a 360° scan, 180 projections, hardware binning of 4, 1,100-ms exposure time, and X-ray source of 80 kV and 500 mA. PET data were reconstructed and quantified using the instrument software (Inveon Acquisition Workplace Version 1.5, Inveon Research Workplace 3.0) in a single 20-min time frame and normalized to the injected dose per body weight. After completion of the PET scan, animals were sacrificed and tissues were sampled as described above.

Pharmacokinetics

Plasma protein binding Frozen plasma samples were thawed and centrifuged for 10 min at 3,000 rpm (1,250 *g*) at 4 °C to remove any precipitates. **BAY 1075553** was diluted in 1 ml plasma to achieve a concentration of 5 MBq/ml. As a control, **BAY 1075553** was diluted in buffer (phosphate-buffered saline, PBS); 400 μl of plasma and controls were transferred to a Microcon 30 ultrafiltration unit (Amicon Inc., Cat. 42410, batch MQB086) and incubated for 30 min at 37 °C in a thermomixer (600 rpm). After incubation a 25-μl aliquot (100 % reference) was collected before centrifuging the ultrafiltration unit at 5,000 *g* (7,170 rpm) for 7 min. A second 25-μl aliquot was obtained from the flow through and compared to the reference sample in a gamma counter.

Plasma stability Freshly prepared human plasma samples were incubated with **BAY 1075553** at a concentration of 5 MBq/ml. Aliquots of 250 μl were incubated at 37 °C for up to 120 min. Incubation in PBS served as control. Plasma proteins were removed by ultrafiltration (Microcon 30 ultrafiltration unit, (Amicon Inc., Cat. 42410, batch MQB086) and subsequently analysed by TLC (10×10 silica gel 60 F254, Merck, Cat: 1.05554.0001; *n*-butanol:acetic acid:water:ethanol=12:3:5:1.5). After running for 60 min the TLC was exposed to a phosphor imaging device (Storm 825, General Electric), and the intensities of the spots quantified by the instrument software.

Microsomes A total of 0.91 MBq **BAY 1075553** was incubated in incubation buffer (50 mM sodium phosphate buffer, pH 7.4) with 25 µl microsome preparation (protein concentration 5 mg/ml) and 50 µl cofactor preparation [glucose-6-phosphate (G6P), Roche, Cat. 127647; $MgCl_2$ Sigma, Cat. M-2670, batch 98H0262; NADP Roche, Cat. 28058; G6P dehydrogenase; Roche, Cat. 127655] for up to 60 min at 37 °C on a thermomixer. Incubations were stopped by adding 500 µl of ice-cooled acetonitrile. After centrifugation for 10 min at 13,000 rpm, the supernatant was analysed by TLC using the same method described in the "plasma stability" section.

Disposition kinetics in rats A total of 10 MBq of **BAY 1075553** was injected i.v. into rats ($n=4$) and blood was sampled via catheterization at different time points (2, 5, 15, 30, 60 and 120 min p.i.) and measured in a gamma counter. For analysis of compound integrity, plasma was prepared and plasma proteins separated by ultrafiltration. Supernatants were subjected to TLC analysis, TLC using the same method described in the "plasma stability" section, for determination of compound integrity.

Dosimetry

Biodistribution in non-tumour-bearing mice was used for dosimetry estimation (see Supplementary Table 2). The total faeces at 3 h p.i. was taken by the sum of faeces and intestinal uptake and used for the gastrointestinal tract model (3.13 % to the small intestine). Two fractions (f1 = 0.73 with a biological half-life of 0.46 h and f2 = 0.17 with a biological half-life of 1.8 h) were calculated via the total body regression fit and used for the urinary bladder model with an assumed voiding interval of 1 h. The number of disintegrations per unit activity administered was calculated by an internal kinetic model by integration of bi-exponential functions. Organ doses were calculated by OLINDA (version 1.1, Vanderbilt University) [38, 39] using the hermaphroditic male and the female model, respectively.

Non-clinical safety studies

All non-clinical safety studies were conducted with the non-radioactive analogue (*rac*)-2-fluoro-4-phosphonomethyl-pentanedioic acid **1**. For in vitro studies, the test compound was dissolved in DMSO. In in vivo studies, physiological saline was used as a vehicle. Doses were selected to give sufficient safety margins to the maximum intended mass dose in a human microdose study. Good Laboratory Practice regulations were applied to all studies relevant for human risk assessment.

In vitro safety pharmacology

hERG potassium channel assay Effects of **1** on hERG potassium channel-mediated current were studied in isolated stably transfected HEK293 cells using the voltage clamp technique according to Himmel [40] at bath concentrations of 0, 1, 10 and 100 µmol/l.

Selectivity Compound **1** was tested for binding activity on a broad panel of targets ($n=68$), such as receptors, ion channels and transporters, at 10 µmol/l. The targets belonged to a safety panel that is known to be associated with adverse drug reactions [41].

In vivo safety pharmacology

Central nervous system Investigation of central nervous system (CNS) function was integrated in the extended single-dose toxicity study (see below). Animals were investigated 15 min, 4 h and 24 h after injection according to the functional observation battery including open field behaviour, motor coordination, locomotive activity, recording of rectal temperature and testing of reflexes.

Cardiovascular function (including ECG) Cardiovascular function was investigated in anaesthetized, artificially ventilated Beagle dogs after consecutive i.v. bolus injections of **1** in a dose range of 0.23–1.15–5.75 mg/kg. Control animals received the vehicle (0.9 % NaCl solution at pH 5) in the same cumulative dosing regimen (3 × 0.5 ml/kg body weight). Each dog received two series of three consecutive i.v. bolus injections (dosing interval 30 min) with escalating doses of **1** and the vehicle. A period of 90 min was between the last injection of the first series and the first injection of the second injection series. After the last injection of the second series an observation period of 90 min followed.

Cardiovascular measurements included arterial blood pressure, heart rate, left ventricular pressure, left ventricular dP/dt, cardiac output, stroke volume and ECG intervals RR, PQ, QRS, QT and QTc (QT interval corrected for heart rate) according to Himmel and Hoffmann [42].

Toxicology

Extended single-dose toxicity An extended single-dose toxicity study (15 animals/sex per group) was performed in Wistar rats with i.v. administration of doses of 0 (vehicle), 0.15, 0.87 and 5.2 mg/kg **1** in saline at an application volume of 5 ml/kg. The animals were sacrificed on days 3 (10 animals/sex per group) and 15 (5 animals/sex per group), respectively. The effects of **1** were assessed by clinical parameters (general observation, food and water consumption, body weight, ophthalmoscopy), clinical pathology (biochemistry, haematology, coagulation, urinalysis) as well as post-mortem examination (gross pathology, organ weight analysis and microscopic examination, including application sites). In addition, testing of

CNS function by means of a functional observational battery and an in vivo micronucleus test in peripheral blood were incorporated into this study.

Genotoxicity Compound **1** was tested for its mutagenic potential in a bacterial reverse mutation test (Ames test, screening assay) in *Salmonella typhimurium* (strains TA100, TA1535, TA102, TA98 and TA1537) in the absence and presence of S-9 mix (derived from liver homogenates of Aroclor 1254-treated male rats) at a maximum dose of 1.0 mg/plate.

Compound **1** was tested in a screening assay in V79 cells for its potential to induce micronuclei in vitro in the absence and presence of S-9 mix at a maximum dose of 500 μg/ml. An in vivo micronucleus test was incorporated into the extended single-dose toxicity study in Wistar rats in subgroups of five animals per sex and group. The frequencies of micronucleated reticulocytes and micronucleated normochromatic erythrocytes were determined by flow cytometry in peripheral blood sampled on days 3 and 4. In addition, the relative reticulocyte counts were determined as a potential indicator of bone marrow toxicity.

Results

Chemistry and radiochemistry

The ^{19}F reference PSMA inhibitors **2** (K_i=1.4 nM), **3** (K_i=3.1 nM) and **5** (K_i=36.4 nM) along with the racemic direct radiolabelling precursors **6** have been described previously [34]. The isomerically pure direct radiolabelling precursors **7**, **8** and **10** were isolated from **6** using preparative chiral HPLC purification methods (Scheme 1; and for details see the "Materials and methods" section).

Radiosyntheses of **BAY 1075553**, **[^{18}F]3** and **[^{18}F]5** (Scheme 2) were performed using methods similar to those described previously for the radiosynthesis of the radiolabelled racemic tracer (**[^{18}F]1**) [34]. The precursors **7**, **8** and **10** were radiolabelled via a nucleophilic radiofluorination reaction to give the intermediates **[^{18}F]11**, **[^{18}F]12** and **[^{18}F]13**, respectively. The ^{18}F-labelled intermediates **[^{18}F]11**, **[^{18}F]12** and **[^{18}F]13** were purified by semi-preparative HPLC, deprotected using strongly acidic conditions (6 M HCl at 120 °C) and subsequently passed through a column of AG11A8 resin (~11 g) and a C18 solid phase extraction cartridge to give the desired products **BAY 1075553**, **[^{18}F]3** and **[^{18}F]5**, respectively, formulated in saline. Extensive investigations were carried out to determine the ratio of stereoisomers in the final formulated solution **BAY 1075553** and to minimize epimerization of the different chiral centres occurring during the harsh radiosynthesis conditions. A novel derivatization method was developed to allow the different stereoisomers to be determined and the final formulated product of **BAY 1075553** was found to contain approximately 10 % of **[^{18}F]3** [32, 35].

In vivo imaging and biodistribution study

BAY 1075553 and stereoisomers **[^{18}F]3** and **[^{18}F]5** thereof were synthesized and used to generate PET/CT images of nude mice bearing prostate cancer tumour xenografts. In accordance with in vitro data [34], only stereoisomers with 4*S* configuration resulted in good visualization of LNCaP xenografts which express high levels of PSMA. Tumour uptake at 50–70 min p.i. was highest for **BAY 1075553** (5.5 ±0.7 %ID/g; n=6, for details see Supplementary Table 1) and the difference compared to the second best stereoisomer **13** was statistically significant (t test; $p<10^{-5}$). At 110–130 min p.i. persistent uptake of **BAY 1075553** (3.8±1.3 %ID/g; n=4) was observed and higher uptake compared to **[^{18}F]3** was maintained. Fast clearance of radioactivity resulted in a low background signal in other organs except for high uptake into kidney and bladder and modest uptake into bone. Kidney

Scheme 1 Synthesis of the radiolabelling precursors

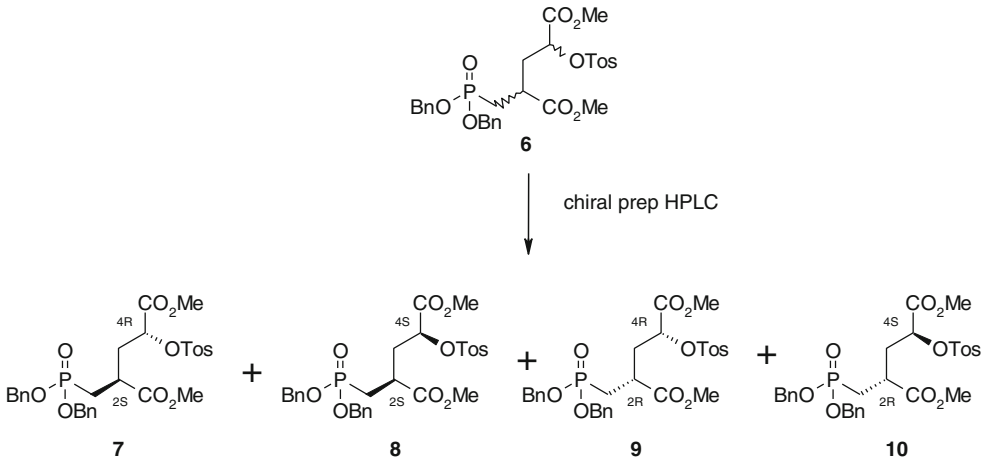

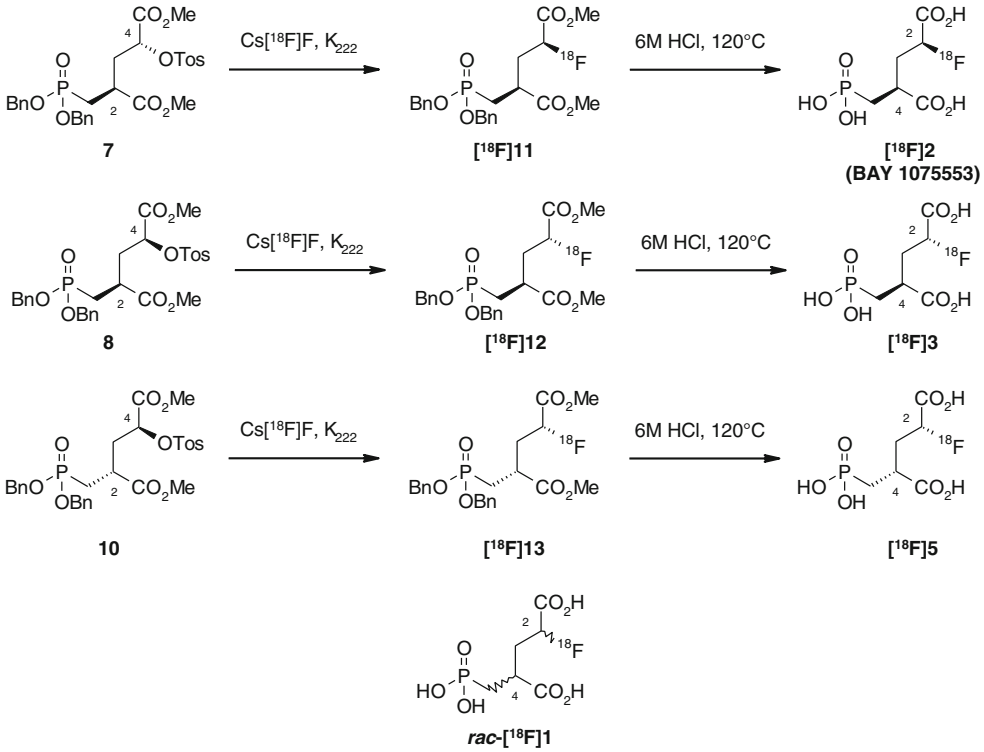

Scheme 2 Radiosynthesis of different stereoisomers of 2-[^{18}F] fluoro-4-phosphonomethyl-pentanedioic acid

uptake of the different isomers correlated with tumour uptake, whereas bone uptake was similar for the three isomers tested and did not increase over time. Exemplified images from this study are shown in Fig. 2 (60 min p.i.) and Fig. 3 (120 min p.i.) as maximum intensity projection (MIP).

To assess tracer uptake immediately p.i., dynamic scans were conducted showing rapid and persistent uptake of **BAY 1075553** into LNCaP tumours within the first minutes after i.v. injection (data not shown).

Besides androgen-dependent LNCaP xenografts, two androgen-independent prostate cancer xenograft models, 22Rv1 expressing PSMA [44] and PC3 lacking PSMA expression [45], were analysed. 22Rv1 tumours were well visualized using **BAY 1075553**, whereas little uptake into PC3 tumours was found (Supplementary Figure 3).

Biodistribution

Biodistribution of **BAY 1075553** was investigated in nude mice bearing subcutaneous LNCaP tumours at four time points (0.5, 1, 2 and 3 h) after i.v. injection of a 250-kBq dose into the tail vein (see Table 1). High and persistent tumour uptake (4–5 %ID/g) over time was found. Tumour to blood (T/B) ratios increased over time with average values of 12.4 at 1 h p.i. and 56 at 3 h p.i. Besides high uptake of **BAY 1075553** into the kidneys (1 h p.i. 41 %ID/g), the only other organs with significant tracer uptake (~2.5 %ID/g) were spleen, bone and adrenals. Predominantly urinary excretion was found with 38 %ID and 64 %ID of radioactivity in the urine after 1 and 2 h, respectively.

Pharmacokinetic characterization

The disposition kinetics was determined in male rats. **BAY 1075553** was administered at a dose of 41 MBq/kg formulated in 0.9 % saline. Radioactivity was measured in blood samples taken from the animals at eight different time points up to 4 h p.i. Pharmacokinetic parameters of the tracer were obtained from total radioactivity corrected with stability data of each blood sample from all animals. The radioactivity time profile of **BAY 1075553** is given in Fig. 4, and a summary of pharmacokinetic parameters is provided in Table 2. **BAY 1075553** was found to be a low clearance compound (0.82 l/h per kg) which is consistent with high metabolic stability/compound integrity. The compound has a short distribution half-life ($T_{1/2}\alpha$ of 5 min) and an elimination half-life $T_{1/2}\alpha$ of 35 min. The volume of distribution was moderate.

Metabolism

The susceptibility of **BAY 1075553** to degradation by phase I oxidative metabolism was investigated using liver microsomes from human, dog, rat and mouse. **BAY 1075553** was stable in all species tested. No metabolic degradation of the tracer was found after 60 min incubation when compared to controls. The extent of plasma protein binding was

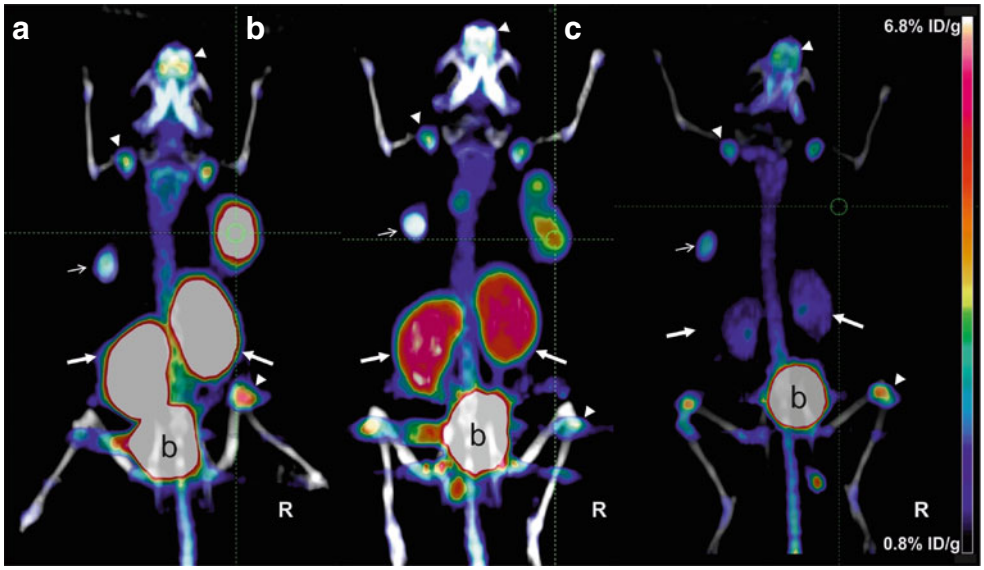

Fig. 2 PET/CT images of different stereoisomers. Human LNCaP prostate tumour-bearing mice were used for tumour visualization by PET. Whole-body PET data (in *rainbow colours*) were acquired 50–70 min p.i. and fused with the CT image (in *grey*). Strong tumour signals (*cross hairs*) were found for **BAY 1075553** (**a**) and **[^{18}F]3** (**b**), whereas tumour uptake was significantly lower for **[^{18}F]5** (**c**). The high background signals observed in bladder (*b*) were due to excretion; besides renal excretion the strong signals in kidneys (*filled arrows*) were caused by specific binding of the tracer to PSMA which is strongly expressed in rodent kidney [14, 43]. Moderate bone uptake (*arrowheads* point to growth plates of skull and long bones) was found but did not increase over time (see Fig. 3). *Open arrows* point to testosterone pellets that were implanted to stimulate growth of the androgen-dependent LNCaP tumour cells. **a** was slightly overblown to allow better comparison with **b** and **c** on the same intensity scale

investigated using plasma from human, rat and dog origin. For all species tested, plasma protein binding of **BAY 1075553** was not detectable. Stability of **BAY 1075553** in human plasma was determined at different time points after incubation. Evaluation of compound integrity was done by TLC. **BAY 1075553** remained stable in human plasma (recovery ≥90 % after 2 h compared to baseline) (Fig. 5). An immobile fraction of **BAY 1075553** was observed in plasma and in PBS controls, co-migrating with free fluoride that increased slightly over time.

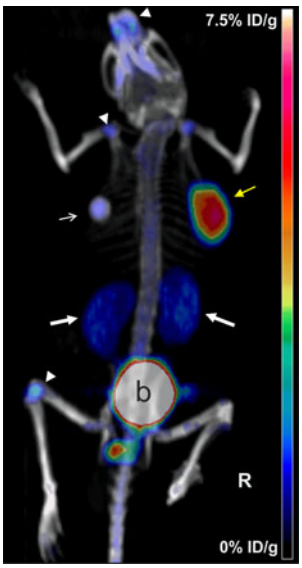

Fig. 3 PET/CT image of **BAY 1075553** 110–130 min p.i. Persistently high tumour uptake (*yellow arrow*) was observed, whereas uptake into kidney (*filled arrows*) and bladder (*b*) decreased compared to earlier time points due to progressing renal elimination of the tracer. For 3-D animation see "Electronic supplementary material"

Dosimetry

Biodistribution of **BAY 1075553** in immunocompetent NMRI mice showed low organ uptake with exception of the kidneys and predominantly urinary excretion. After 3 h about 79 % of the injected dose was excreted into the urine and about 3 % was excreted via the hepatobiliary pathway. Highest organ doses in the hermaphroditic male model were found for kidneys (0.252 mGy/MBq) and the urinary bladder wall (0.180 mGy/MBq). They were also the main contributors to the effective dose (ED) of 0.0219 mSv/MBq. The same dose-receiving organs in terms of total dose and ED contribution were found for the female model (ED 0.0246 mSv/MBq) (Table 3).

Safety pharmacology

Compound **1** showed no binding activity on a broad panel of receptors, ion channels and transporters [41] at 10 μmol/l in vitro. Furthermore, **1** had no effect on the hERG potassium

Table 1 Biodistribution of **BAY 1075553** in LNCaP-bearing nude mice ($n=3$ per time point)

%Dose/g	0.5 h		1 h		2 h		3 h	
		SD		SD		SD		SD
Spleen	3.00	0.48	2.48	0.26	0.42	0.19	0.41	0.06
Liver	0.40	0.06	0.42	0.06	0.24	0.04	0.35	0.07
Kidney	105.78	24.49	104.40	6.10	41.15	16.38	46.96	23.92
Lung	1.12	0.04	0.49	0.22	0.17	0.07	0.16	0.03
Bone	2.61	0.35	2.53	0.26	1.52	0.33	2.12	0.48
Heart	0.53	0.01	0.27	0.06	0.06	0.02	0.08	0.01
Brain	0.05	0.01	0.06	0.02	0.04	0.02	0.03	0.01
Fat	0.78	0.15	0.36	0.08	0.17	0.09	0.35	0.17
Thyroid	0.68	0.13	0.45	0.11	0.18	0.04	0.30	0.07
Testes	0.76	0.19	0.50	0.02	0.15	0.01	0.20	0.01
Muscle	0.26	0.14	0.21	0.05	0.12	0.12	0.06	0.02
Tumour	5.31	1.83	4.08	1.24	3.13	0.54	4.54	0.93
Skin	0.85	0.01	0.76	0.20	0.29	0.06	0.24	0.04
Blood	0.79	0.05	0.33	0.12	0.07	0.02	0.08	0.02
Tail	4.69	1.55	2.37	1.01	1.73	0.09	2.52	0.68
Stomach	0.51	0.05	0.26	0.06	0.11	0.03	0.20	0.05
Prostate	0.69	0.26	0.70	0.15	0.66	0.95	0.53	0.29
Intestine	0.23	0.01	0.23	0.08	0.28	0.16	1.03	0.80
Pancreas	0.45	0.10	0.22	0.04	0.07	0.01	0.09	0.02
Adrenals	3.31	0.46	2.46	0.36	0.51	0.31	0.57	0.17
Excretion %ID		SD		SD		SD		SD
Urine	26.4	5.89	38.84	9.01	64.14	7.76	59.84	10.41
Faeces	0.20	0.33	0.14	0.12	1.23	1.18	1.13	1.77

tail current up to concentrations of 100 µmol/l. The overall results of the in vivo safety pharmacology studies with **1** revealed no dose-related effects on peripheral and CNS function in rats up to the high dose of 5.2 mg/kg. Moreover, in dogs, no effects on cardiovascular function (including ECG) and no obvious risk for QT prolongation in humans were seen up to the highest dose of 5.75 mg/kg.

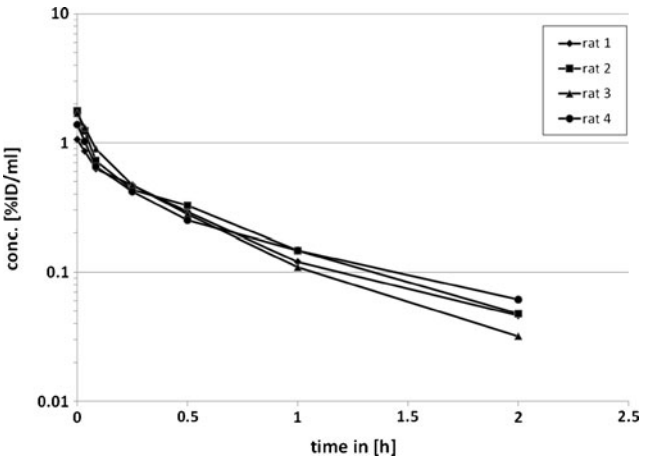

Fig. 4 Radioactivity time profile of **BAY 1075553** after i.v. administration to Wistar rats

Toxicology

The extended single-dose study in Wistar rats with i.v. administration corresponding to the intended human route of administration revealed no compound-related effects The high dose of 5.2 mg/kg **1** was identified as the no observed effect level (NOEL), corresponding to 1.8 mg/kg of **2** and 0.79 mg/kg of **3**. No evidence for a mutagenic potential of the compound was found in vitro and in vivo (for details refer to the "Materials and methods" section).

Discussion

The PSMA inhibitor scaffolds explored by other groups for radiolabelling with SPECT and PET radioisotopes can be approximately split into three categories: (1) glutamate-urea heterodimers, (2) glutamate-containing phosphoramidates and (3) 2-(phosphinylmethyl)pentanedioic acid [27–31, 47–49]. The majority of published work focused on the glutamate-urea heterodimer scaffold after the first promising results obtained with *N*-[*N*-[(*S*)-1,3-dicarboxypropyl]carbamoyl]-*S*-[^{11}C]methyl-L-cysteine ([^{11}C]DCMC) and *N*-[*N*-[(*S*)-1,3-dicarboxypropyl]carbamoyl]-*S*-3-[^{125}I]iodo-L-tyrosine

Table 2 Pharmacokinetic parameters of **BAY 1075553** after single i.v. administration

Species Dose	MBq/kg	Rat 1 41	Rat 2 43	Rat 3 43	Rat 4 38	Mgeo	SDgeo
CL_{blood}	l/h kg	0.87	0.77	0.84	0.79	0.82	1.1
V_{ss}	l/kg	0.63	0.53	0.46	0.71	0.58	1.2
$T_{1/2\ \alpha}$	h	0.11	0.065	0.091	0.077	0.085	1.3
Interval[a]	h	0.03–0.083	0.03–0.083	0.03–0.083	0.03–0.083		
$T_{1/2\beta}$	h	0.58	0.55	0.49	0.75	0.59	1.2
Interval[a]	h	0.5–2	0.5–2	0.5–22	0.5–2		

Mgeo geometric mean, *SDgeo* geometric standard deviation

[a] Used for regression to determine half-life

([^{125}I]DCIT) [47]. Presently the glutamate-urea-lysine heterodimer seems to be the heterodimer of choice with subnanomolar binding affinity and impressive preclinical in vivo images being reported with different radioisotopes, i.e. ^{18}F [28], ^{68}Ga [27], ^{123}I [30], ^{131}I [30], ^{188}Re [49] and ^{99m}Tc [49].

We have previously reported that (2*S*,4*S*)-2-fluoro-4-(phosphonomethyl)-pentanedioic acid and (2*R*,4*S*)-2-fluoro-4-(phosphonomethyl)-pentanedioic acid are highly potent inhibitors of PSMA and that the ^{18}F-radiolabelled racemic analogue 2-[^{18}F]fluoro-4-(phosphonomethyl)-pentanedioic acid (**[^{18}F]1**) clearly visualizes the tumour in LNCaP tumour-bearing mice [34]. Here we report in detail the preclinical performance of **BAY 1075553** including microPET/CT imaging, biodistribution, dosimetry estimates, pharmacokinetics, toxicological and safety pharmacological studies as a prerequisite for initial clinical testing in prostate cancer patients.

Based on our previous observations [34], we hypothesized that radiosyntheses of the stereoisomers with 4*S* configuration might further improve the imaging performance in comparison to the racemic mixture of 2-[^{18}F]fluoro-4-(phosphonomethyl)-pentanedioic acid (*rac*-[^{18}F]-**1**).

In order to test this hypothesis we separated the different isomers from the racemic precursor **6** [34] using preparative chiral HPLC and characterized the individual isomerically pure direct radiolabelling precursors **7**–**10**.

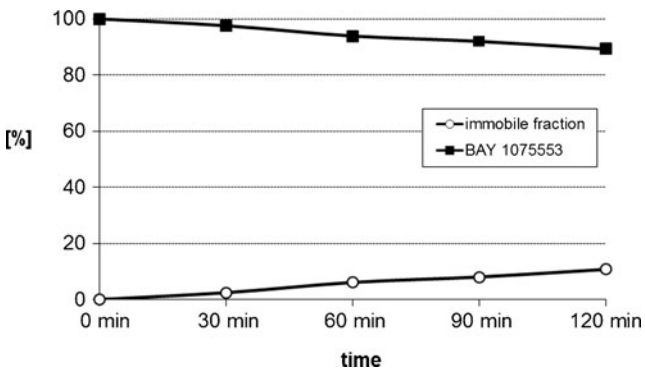

Fig. 5 Recovery of intact **BAY 1075553** at different time points after incubation in human plasma

Radiofluorination of the precursors **7**, **8** and **10**, subsequent purification and formulation were essentially carried out using the same methodology published previously [34]. The only major difference was that the radiofluorination step for the isomerically pure precursors used cesium carbonate and not potassium carbonate, as this step was monitored with respect to epimerization of the carbon containing the tosylate leaving group, and cesium carbonate was found to minimize

Table 3 Projected human organ doses and effective doses of **BAY 1075553**

Target organ	Organ dose (mGy/MBq)	ED (mSv/MBq)
Adrenals	1.23E-02	3.08E-05
Brain	7.66E-04	1.92E-06
Breasts	2.85E-03	1.42E-04
Gallbladder wall	9.05E-03	0.00E+00
LLI wall	1.30E-02	1.56E-03
Small intestine	1.84E-02	4.59E-05
Stomach wall	6.67E-03	8.01E-04
ULI wall	1.92E-02	4.79E-05
Heart wall	3.25E-03	0.00E+00
Kidneys	2.52E-01	6.30E-03
Liver	5.86E-03	2.93E-04
Lungs	3.02E-03	3.62E-04
Muscle	5.55E-03	1.39E-05
Ovaries	1.08E-02	2.16E-03
Pancreas	9.60E-03	2.40E-05
Red marrow	5.97E-03	7.17E-04
Osteogenic cells	6.19E-03	6.19E-05
Skin	3.42E-03	3.42E-05
Spleen	1.02E-02	2.54E-05
Testes	9.63E-03	0.00E+00
Thymus	3.40E-03	8.51E-06
Thyroid	3.92E-03	1.96E-04
Urinary bladder wall	1.80E-01	8.99E-03
Uterus	1.67E-02	4.16E-05
Carcass	6.58E-03	0.00E+00
ED (mSv/MBq)	–	2.19E-02

LLI lower large intestine, *ULI* upper large intestine

this epimerization (data not shown). To determine the ratio of the individual stereoisomers in the final formulated radiotracer solution, we developed a fast, quantitative derivatization method that allowed this ratio to be determined [36, 37]. The results from this derivatization method showed that the radiolabelling of precursor **7** gave a mixture of the (2*S*,4*S*)-isomer (**[^{18}F]2**; ~90 %) and the corresponding (2*R*,4*S*)-isomer (**[^{18}F]3**; ~10 %) in the final formulated solution ([37]). This mixture is referred herein to as **BAY 1075553**. Similar epimerizations resulting from the harsh radiolabelling conditions have been reported previously for: (1) *cis*-4[^{18}F]fluoro-L-proline, where despite having a stereochemically pure precursor, the range of the undesired *trans*-isomer varied from 7.1 to 28.8 % [50], and (2) 4-[^{18}F]fluoroglutamate where the stereochemically pure precursor gave only 58.3 % of the desired S_N2-stereoisomer [51].

These well characterized radiopreparations allowed us to compare **BAY 1075553** with **[^{18}F]3** and **[^{18}F]5** in LNCaP prostate cancer xenografts that express high levels of PSMA. While no uptake was detectable for **[^{18}F]5**, both **BAY 1075553** and **[^{18}F]3** showed good visualization of the LNCaP xenografts. However, uptake of **BAY 1075553** was significantly higher compared to **[^{18}F]3**. These results are in line with our previous results in vitro where we showed that the (2*S*,4*S*)- and (2*R*,4*S*)-isomers of 2-fluoro-4-(phosphonomethyl)-pentanedioic acid (**2** and **3**) are highly potent inhibitors of PSMA with binding affinities (K_i) of 1.4 nM and 3.1 nM, respectively [34]. Based on these results we focused further studies on **BAY 1075553**.

In in vivo studies, employing biodistribution and PET imaging, **BAY 1075553** showed specific and effective targeting of PSMA-positive prostate cancer xenografts (LNCap, 22RV1). The image quality obtained with **BAY 1075553** in the LNCaP tumour model compares favourably with preclinical results published previously using an ^{18}F-labelled radiotracer targeting PSMA inhibitor [29, 31]. Since PSMA expression in 22RV1 cells has been estimated to be tenfold less compared to LNCaP cells [44] **BAY 1075553** was capable of detecting even these low-expressing prostate tumours. Rapid tumour targeting and fast and almost exclusively renal excretion was found. More detailed pharmacokinetic analyses characterized **BAY 1075553** as a low clearance compound (0.82 l/h per kg), which is consistent with its high metabolic stability/compound integrity observed in serum and microsomes. The distribution half-life ($T_{1/2}\alpha$ of 5 min) and an elimination half-life $T_{1/2}\alpha$ of 35 min were short allowing fast elimination of the compound p.i. The renal elimination route contributed to the high uptake found in kidney and bladder of the animals. However, kidney uptake of the tested isomers differed and correlated with tumour uptake pointing to specific binding of the tracer to its target in this organ which is in line with previous observations reporting high PSMA expression in rodent kidneys [14, 43]. Compared to rodents, expression of PSMA in the human kidney was reported to be less pronounced [21]. PSMA was also reported to be expressed in brain and in intestinal brush border membranes [21], but in our preclinical models no substantial uptake was found in these organs. These findings may be explained by low accessibility of our highly polar compound to the brain and expression of PSMA on the luminal side of the intestinal brush border membrane which might be less accessible to the PET tracer.

BAY 1075553 uptake found in bone (~2.5 %ID/g at 60 min p.i.) was strongest in regions of active bone growth in skull and long bones, but did not increase over time (see Table 1). Therefore, we concluded that bone uptake was not due to increasing fluoride incorporation upon compound disintegration in vivo but rather due to specific compound binding to bone structures. Since expression of PSMA in bone structures was not detectable [14, 19], binding of **BAY 1075553** may be independent of PSMA expression and might be explained by **BAY 107553**'s phosphonate structure. Our finding that the inactive stereoisomer **[^{18}F]5** showed similar bone uptake compared to **BAY 1075553** (see Fig. 1) further supports this hypothesis. The observed bone uptake, if confirmed in human prostate cancer patients, may interfere with diagnostic applications evaluating bone metastases, while imaging of the primary tumour and of lymph node and soft tissue metastases would not be affected. If this profile of diagnostic applications is confirmed in prostate cancer patients, **BAY 1075553** may well complement choline-based tracers in the clinic, which have recently been approved for metastatic prostate cancer, but use in detection of primary prostate cancer and lymph node metastases remains controversial [52].

To support a potential first-in-human study we have explored radiation safety and drug safety aspects. We predicted the radiation burden for human application based on biodistribution data originating from non-tumour-bearing mice for **BAY 1075553** and conducted dosimetry calculations using OLINDA version 1.1 [38]. We found highest organ doses for the kidneys (0.252 mGy/MBq) and the urinary bladder wall (0.180 mGy/MBq) and these were the main contributors to the ED which was calculated with 0.0219 mSv/MBq. Based on these estimates and assuming a 300 MBq dose, a radiation dose of 6.6 mSv is predicted for a PET scan using **BAY 1075553** in patients which is comparable with the radiation dose of a routine [^{18}F]FDG PET scan (0.019 mSv/MBq) [46]. This calculation has not taken into consideration the lower expression of PSMA in human kidney compared to rodents mentioned above, which might result in lower exposure of the tracer in humans.

Non-clinical safety studies in rats and dogs were conducted with **1**, the racemic, non-radioactive analogue of the active ^{18}F-labelled **BAY 1075553**. These species are regarded as relevant for non-clinical safety assessment to support human clinical trials since similar potency of **2** for inhibition of NAALAdase activity from rat and dog brain as compared to

human LNCaP cells was observed (unpublished data). Furthermore, assessment of metabolic stability of **BAY 1075553** in liver microsomes did not reveal any species differences.

Non-clinical safety studies did not reveal any off-target activities in the in vitro and in vivo studies conducted. The respective highest tested in vivo doses in dogs and rats correspond to >1,000-fold of a potential maximum human mass dose of 100 μg **BAY 1075553** per volunteer, the highest possible dose in a clinical microdose study according to the international guideline ICH M3 [53].

Conclusion

BAY 1075553 was identified as a novel PET tracer binding to PSMA, a well characterized target for prostate cancer imaging. Biodistribution and microPET/CT imaging experiments showed high tumour uptake, low background in other organs as well as fast and exclusively renal elimination in mice bearing PSMA-positive tumours. **BAY 1075553** can be produced using a robust, direct radiosynthesis procedure and quality control procedures for the production including isomeric contribution were established. As a prerequisite for translating **BAY 1075553** into clinical testing we have conducted detailed pharmacokinetic, toxicological and safety pharmacological studies, the results of which have supported regulatory approval for testing **BAY 1075553** in a first-in-man microdose study with single i.v. administration in prostate cancer patients, preliminary results of which have already been presented [54, 55].

Acknowledgments We would like to acknowledge the excellent technical support of Selahattin Ede, Marion Zerna, Mario Mandau, Oliver Schenk, Uwe Rettig, Yvonne Duchstein, Eva-Maria Bickel, Jörg Jannsen, Herbert Himmel, and Michael Hoffmann. This work was conducted at and financially supported by Bayer Healthcare.

Conflicts of interest All authors are or were employees of Bayer Healthcare.

References

1. Jemal A, Siegel R, Xu J, Ward E. Cancer statistics, 2010. CA Cancer J Clin. 2010;60:277–300.
2. Rinnab L, Simon J, Hautmann RE, Cronauer MV, Hohl K, Buck AK, et al. [(11)C]choline PET/CT in prostate cancer patients with biochemical recurrence after radical prostatectomy. World J Urol. 2009;27:619–25.
3. Beheshti M, Vali R, Waldenberger P, Fitz F, Nader M, Loidl W, et al. Detection of bone metastases in patients with prostate cancer by 18F fluorocholine and 18F fluoride PET-CT: a comparative study. Eur J Nucl Med Mol Imaging. 2008;35:1766–74.
4. Kotzerke J, Volkmer BG, Glatting G, van den Hoff J, Gschwend JE, Messer P, et al. Intraindividual comparison of [11C]acetate and [11C]choline PET for detection of metastases of prostate cancer. Nuklearmedizin. 2003;42:25–30.
5. Castellucci P, Fuccio C, Nanni C, Santi I, Rizzello A, Lodi F, et al. Influence of trigger PSA and PSA kinetics on 11C-choline PET/CT detection rate in patients with biochemical relapse after radical prostatectomy. J Nucl Med. 2009;50:1394–400.
6. Iason. IASOcholine 1,0 GBq/ml, Injektionslösung, Fachinformation Deutschland. [http://www.iason.eu/fileadmin/user_upload/SPC/iasocholine%20germany.pdf].
7. Gambhir SS, Czernin J, Schwimmer J, Silverman DH, Coleman RE, Phelps ME. A tabulated summary of the FDG PET literature. J Nucl Med. 2001;42:1S–93.
8. Oyama N, Akino H, Suzuki Y, Kanamaru H, Sadato N, Yonekura Y, et al. The increased accumulation of [18F]fluorodeoxyglucose in untreated prostate cancer. Jpn J Clin Oncol. 1999;29:623–9.
9. Schwarzenbock S, Souvatzoglou M, Krause BJ. Choline PET and PET/CT in primary diagnosis and staging of prostate cancer. Theranostics. 2012;2:318–30.
10. Sutinen E, Nurmi M, Roivainen A, Varpula M, Tolvanen T, Lehikoinen P, et al. Kinetics of [(11)C]choline uptake in prostate cancer: a PET study. Eur J Nucl Med Mol Imaging. 2004;31:317–24.
11. Li Y, Cozzi PJ, Russell PJ. Promising tumor-associated antigens for future prostate cancer therapy. Med Res Rev. 2010;30:67–101.
12. Horoszewicz JS, Kawinski E, Murphy GP. Monoclonal antibodies to a new antigenic marker in epithelial prostatic cells and serum of prostatic cancer patients. Anticancer Res. 1987;7:927–35.
13. Wright Jr GL, Haley C, Beckett ML, Schellhammer PF. Expression of prostate-specific membrane antigen in normal, benign, and malignant prostate tissues. Urol Oncol. 1995;1:18–28.
14. Silver DA, Pellicer I, Fair WR, Heston WD, Cordon-Cardo C. Prostate-specific membrane antigen expression in normal and malignant human tissues. Clin Cancer Res. 1997;3:81–5.
15. Sweat SD, Pacelli A, Murphy GP, Bostwick DG. Prostate-specific membrane antigen expression is greatest in prostate adenocarcinoma and lymph node metastases. Urology. 1998;52:637–40.
16. Bostwick DG, Pacelli A, Blute M, Roche P, Murphy GP. Prostate specific membrane antigen expression in prostatic intraepithelial neoplasia and adenocarcinoma: a study of 184 cases. Cancer. 1998;82:2256–61.
17. Wright Jr GL, Grob BM, Haley C, Grossman K, Newhall K, Petrylak D, et al. Upregulation of prostate-specific membrane antigen after androgen-deprivation therapy. Urology. 1996;48:326–34.
18. Chang SS, Gaudin PB, Reuter VE, Heston WD. Prostate-specific membrane antigen: present and future applications. Urology. 2000;55:622–9.
19. Ananias HJ, van den Heuvel MC, Helfrich W, de Jong IJ. Expression of the gastrin-releasing peptide receptor, the prostate stem cell antigen and the prostate-specific membrane antigen in lymph node and bone metastases of prostate cancer. Prostate. 2009;69:1101–8.
20. Mannweiler S, Amersdorfer P, Trajanoski S, Terrett JA, King D, Mehes G. Heterogeneity of prostate-specific membrane antigen (PSMA) expression in prostate carcinoma with distant metastasis. Pathol Oncol Res. 2009;15:167–72.
21. Mhawech-Fauceglia P, Zhang S, Terracciano L, Sauter G, Chadhuri A, Herrmann FR, et al. Prostate-specific membrane antigen (PSMA) protein expression in normal and neoplastic tissues and its sensitivity and specificity in prostate adenocarcinoma: an immunohistochemical study using mutiple tumour tissue microarray technique. Histopathology. 2007;50:472–83.
22. Mease RC. Radionuclide based imaging of prostate cancer. Curr Top Med Chem. 2010;10:1600–16.
23. Tagawa ST, Milowsky MI, Morris MJ, Vallabhajosula S, Christos PJ, Akhtar NH, et al. Phase II study of lutetium-177 labeled anti-prostate-specific membrane antigen (PSMA) monoclonal antibody J591 for metastatic castration-resistant prostate cancer. Clin Cancer Res. 2013.
24. Holland JP, Divilov V, Bander NH, Smith-Jones PM, Larson SM, Lewis JS. 89Zr-DFO-J591 for immunoPET of prostate-specific membrane antigen expression in vivo. J Nucl Med. 2010;51:1293–300.

25. Robinson MB, Blakely RD, Couto R, Coyle JT. Hydrolysis of the brain dipeptide N-acetyl-L-aspartyl-L-glutamate. Identification and characterization of a novel N-acetylated alpha-linked acidic dipeptidase activity from rat brain. J Biol Chem. 1987;262:14498–506.
26. Slusher BS, Vornov JJ, Thomas AG, Hurn PD, Harukuni I, Bhardwaj A, et al. Selective inhibition of NAALADase, which converts NAAG to glutamate, reduces ischemic brain injury. Nat Med. 1999;5:1396–402.
27. Banerjee SR, Pullambhatla M, Byun Y, Nimmagadda S, Green G, Fox JJ, et al. 68Ga-labeled inhibitors of prostate-specific membrane antigen (PSMA) for imaging prostate cancer. J Med Chem. 2010;53:5333–41.
28. Chen Y, Foss CA, Byun Y, Nimmagadda S, Pullambhatla M, Fox JJ, et al. Radiohalogenated prostate-specific membrane antigen (PSMA)-based ureas as imaging agents for prostate cancer. J Med Chem. 2008;51:7933–43.
29. Lapi SE, Wahnishe H, Pham D, Wu LY, Nedrow-Byers JR, Liu T, et al. Assessment of an 18F-labeled phosphoramidate peptidomimetic as a new prostate-specific membrane antigen-targeted imaging agent for prostate cancer. J Nucl Med. 2009;50:2042–8.
30. Maresca KP, Hillier SM, Femia FJ, Keith D, Barone C, Joyal JL, et al. A series of halogenated heterodimeric inhibitors of prostate specific membrane antigen (PSMA) as radiolabeled probes for targeting prostate cancer. J Med Chem. 2009;52:347–57.
31. Mease RC, Dusich CL, Foss CA, Ravert HT, Dannals RF, Seidel J, et al. N-[N-[(S)-1,3-Dicarboxypropyl]carbamoyl]-4-[18F]fluorobenzyl-L-cysteine, [18F]DCFBC: a new imaging probe for prostate cancer. Clin Cancer Res. 2008;14:3036–43.
32. Barrett JA, Coleman RE, Goldsmith SJ, Vallabhajosula S, Petry NA, Cho S, et al. First-in-man evaluation of 2 high-affinity PSMA-avid small molecules for imaging prostate cancer. J Nucl Med. 2013;54:380–7.
33. Cho SY, Gage KL, Mease RC, Senthamizhchelvan S, Holt DP, Jeffrey-Kwanisai A, et al. Biodistribution, tumor detection, and radiation dosimetry of 18F-DCFBC, a low-molecular-weight inhibitor of prostate-specific membrane antigen, in patients with metastatic prostate cancer. J Nucl Med. 2012;53:1883–91.
34. Graham K, Lesche R, Gromov AV, Böhnke N, Schäfer M, Hassfeld J, et al. Radiofluorinated derivatives of 2-(phosphonomethyl) pentanedioic acid as inhibitors of prostate specific membrane antigen (PSMA) for the imaging of prostate cancer. J Med Chem. 2012;55:9510–20.
35. Graham K, Lesche R, Gromov AV, Böhnke N, Hassfeld J, Kettschau G. Prostate specific membrane antigen inhibitors. Patent WO 2011/073286, 2011.
36. Graham K, Ede S. Derivatization of radiopharmaceuticals. Patent WO2012/104225, 2012.
37. Graham K, Kettschau G, Gromov A, Dinkelborg L. Development of a fast robust derivatization method of an extremely polar PET radiopharmaceutical; a critical aspect for starting a clinical trial. Tetrahedron Lett. 2013;54:2583–6.
38. Stabin MG, Siegel JA. Physical models and dose factors for use in internal dose assessment. Health Phys. 2003;85:294–310.
39. Stabin MG, da Luz LC. Decay data for internal and external dose assessment. Health Phys. 2002;83:471–5.
40. Himmel HM. Suitability of commonly used excipients for electrophysiological in-vitro safety pharmacology assessment of effects on hERG potassium current and on rabbit Purkinje fiber action potential. J Pharmacol Toxicol Methods. 2007;56:145–58.
41. Hamon J, Whitebread S, Techer-Etienne V, Le Coq H, Azzaoui K, Urban L. In vitro safety pharmacology profiling: what else beyond hERG? Future Med Chem. 2009;1:645–65.
42. Himmel HM, Hoffmann M. QTc shortening with a new investigational cancer drug: a brief case study. J Pharmacol Toxicol Methods. 2010;62:72–81.
43. Tsai G, Slusher BS, Sim L, Coyle JT. Immunocytochemical distribution of N-acetylaspartylglutamate in the rat forebrain and glutamatergic pathways. J Chem Neuroanat. 1993;6:277–92.
44. Hillier SM, Kern AM, Maresca KP, Marquis JC, Eckelman WC, Joyal JL, et al. 123I-MIP-1072, a small-molecule inhibitor of prostate-specific membrane antigen, is effective at monitoring tumor response to taxane therapy. J Nucl Med. 2011;52:1087–93.
45. Ghosh A, Wang X, Klein E, Heston WD. Novel role of prostate-specific membrane antigen in suppressing prostate cancer invasiveness. Cancer Res. 2005;65:727–31.
46. Radiation dose to patients from radiopharmaceuticals (addendum 2 to ICRP publication 53). Ann ICRP. 1998;28:1–126.
47. Foss CA, Mease RC, Fan H, Wang Y, Ravert HT, Dannals RF, et al. Radiolabeled small-molecule ligands for prostate-specific membrane antigen: in vivo imaging in experimental models of prostate cancer. Clin Cancer Res. 2005;11:4022–8.
48. Misra P, Humblet V, Pannier N, Maison W, Frangioni JV. Production of multimeric prostate-specific membrane antigen small-molecule radiotracers using a solid-phase 99mTc preloading strategy. J Nucl Med. 2007;48:1379–89.
49. Banerjee SR, Foss CA, Castanares M, Mease RC, Byun Y, Fox JJ, et al. Synthesis and evaluation of technetium-99m- and rhenium-labeled inhibitors of the prostate-specific membrane antigen (PSMA). J Med Chem. 2008;51:4504–17.
50. Hamacher K. Synthesis of N.C.A. cis- and trans-4-[18F]fluoro-l-proline, radiotracers for PET-investigation of disordered matrix protein synthesis. J Labelled Comp Radiopharm. 1999;42:1135–44.
51. Krasikova RN, Kuznetsova OF, Fedorova OS, Belokon YN, Maleev VI, Mu L, et al. 4-[18F]fluoroglutamic acid (BAY 85–8050), a new amino acid radiotracer for PET imaging of tumors: synthesis and in vitro characterization. J Med Chem. 2011;54:406–10.
52. Zengerling F, Schrader AJ, Schrader M, Jentzmik F. Diagnostic relevance of choline-PET/CT in patients with prostate cancer. Aktuelle Urol. 2012;43:49–54.
53. EMEA. Guidance on non-clinical safety studies for the conduct of human clinical trials and marketing authorization for pharmaceuticals, CPMP/ICH/286/95. 2009.
54. Langsteger W, Kunit T, Haim S, Nader M, Valencia R, Lesche R, et al. BAY 1075553 PET/CT in the assessment of prostate cancer: safety, tolerability and biodistribution—phase I first in human study results. J Nucl Med. 2012;53(Suppl 1):1125.
55. Beheshti M, Langsteger W, Sommerhuber A, Steinmair M, Wolf I, Valencia R, et al. BAY 1075553 PET/CT in staging and re-staging of prostate cancer patients—phase I study and comparison to 18F-FCH. J Nucl Med. 2012;53(Suppl 1):272.